Deposition of polycrystalline and nanocrystalline diamond on graphite

Deposition of polycrystalline and nanocrystalline diamond on graphite: effects of surface pre-treatments

I. Villalpando,[*a1] P. John,[a] S. Porro[a2] and J. I. B. Wilson[a]

[a]*School of Engineering and Physical Sciences, Heriot-Watt University, Riccarton, Edinburgh, EH14 4AS, UK. E-mail:I.Villalpando@cirena.org, Fax + 52 629 534 6023, Tel. +52 629 534 6048*

Abstract

The growth of hydrogenated sp^3-phase of diamond on the sp^2-phase of graphite by Microwave Plasma Enhanced Chemical Vapour Deposition (MPECVD) is a challenge, primarily because hydrogen etches graphite much faster than the growth rate of diamond. In order to enhance nucleation of diamond on graphite we used a plethora of techniques such as plasma etching, ion bombardment, manual scratching and scratching by ultrasonic agitation. Nanocrystalline and polycrystalline diamond thin-films were grown by MPECVD on the surface of pre-treated or pristine graphite using 1.5, 3.0 and 3.6kW microwave power. Samples were characterised by Scanning Electron Microscopy, Raman Spectroscopy and X-ray Photoelectron Spectroscopy. Species in the gas phase during film deposition were monitored by Optical Emission Spectroscopy. We have found that the surface area covered and the morphology of the diamond films are dependent on the surface pre-treatment. The crystallite size of the films depends on the microwave power used during MPECVD growth. The results of this study establish the protocols for diamond deposition by MPECVD on graphite substrates with a desired crystalline quality based on the pre-treatment of the substrate and the microwave power used during MPECVD. These results are important to modern applications such as plasma facing materials in which diamond has shown outstanding performance in contrast to that of graphite.

Keywords: Diamond growth, graphite, nucleation, CVD

1 Introduction

Today graphite materials are some of the preferred candidates for the inside of tokamak chambers for fusion application, however erosion and tritium retention still limit their use. Diamond thin films have shown good perfomance when exposed to extreme conditions such as high power plasmas [1]. The use of diamond coatings on graphite is a good alternative to face the plasma in tokamak chambers. In previous work we have shown diamond performance at high plasma etching conditions and in this work the results are focussed on diamond thin films preparations to achive a desired morphology. In the growth of diamond films on non-diamond surfaces it is common practice to pre-treat the substrate

1.Present address: Centro de Investigación para los Recursos Naturales, Antigua Normal Rural de Salaices, López, Chihuahua, México, C.P. 33941

2 Present address:Department of Applied Science and Technology, Politecnico di Torino, Corso Duca degli Abruzzi 24, 10129 Torino, Italy

to increase diamond nucleation: this step is important because nucleation density influences the growth rate [2], the film quality [3], and the film morphology [4]. Traditionally, nucleation pre-treatments achieve diamond growth on substrates where nucleation is difficult to start because of the surface smoothness, such as mirror polished wafers (in which case a simple scratching is sufficient [5]) or to increase adhesion to the substrates (such as etching procedures and intermediate layers on hard metal surfaces [6]) for specific application such as cutting tools. Pre-treatments to achieve high nucleation densities have also been used to increase the surface area covered by the film and enhance adhesion that is fundamental in applications such as plasma facing materials for extreme environments such as fusion reactors [7-9].

Diamond grows three dimensionally in a Volmer-Weber growth mode [10], that is, crystals grow until they coalesce to form a film. If the nucleation density is low, the surface coverage is poor resulting in a porous film combined with a rough surface comprising micron sized crystallites. The selection of nucleation pre-treatment will depend on the specific application of the diamond film, but also on the substrate, and a detailed study of nucleation conditions is needed before growing on non-conventional materials such as graphite. There is a lack of information on the growth of diamond on graphite by Microwave Plasma Enhanced Chemical Vapour Deposition (MPECVD) because hydrogen etches graphite much faster than diamond grows [11]. Angus and co-workers published a series of seminal papers on the hydrogenation of graphite [12, 13, 14]. They suggested that hydrogenation occurs preferentially at the edges of graphite planes, transforming the unsaturated rings into their fully saturated analogues. In low pressure diamond growth environments, the saturated rings result in diamond nucleation or even conversion to diamond. In this way diamond nucleation should proceed without the need of external seeding or scratching pre-treatments. Chow et al. [15] and Regel et al. [16] had also grown diamond on graphite in a hot filament system without nucleation pre-treatment.

This study intends to establish diamond nucleation conditions on graphite substrates and to evaluate the morphology and purity of the resulting films. The surfaces of graphite were treated using techniques conventionally used for non-diamond substrates [17, 18] and the resulting films are compared.

We have seen that nucleation pre-treatments on graphite substrates increase the area covered by the film, control the morphology and increase the quality, which are fundamental requirements for modern applications such as plasma facing materials for fusion reactors.

2 Experimental

Samples of 20x20x3mm^3 highly oriented pyrolytic graphite (HOPG) pieces (supplied by Ringsdorff Werke GmbH, Bonn, Germany) were cleaned with methanol in an ultrasonic bath before one of the different nucleation processes was applied, and one control sample was kept untreated for growth on a pristine graphite substrate (sample A). The nucleation techniques used in this study were selected after a bibliographic review; such processes being the most

frequently used and the most efficient for growing diamond on different kinds of substrates ([19] is a good review of diamond nucleation treatments). Three samples were ultrasonically scratched for 30 min with a maximum power of 120W (Bandelin Sonorex Digital 10P ultrasonic bath) to ensure homogeneous surface abrasion of each of the substrates by one of the three diamond powder suspensions used: 3% micro-diamond in methanol (sample H), (~1 µm natural diamond, De Beers), or nanodiamond (sample B) (previously cleaned following the method described by Jiang and Xu [20]), or a mixture of micro-diamond plus titanium (sample C) (100 mesh, 99.7% Sigma-Aldrich). After the ultrasonic treatment, samples were rinsed in methanol and dried in vacuum.

One further sample was treated by manual scratching using a methanol slurry of micro-diamond powder for 2 min (sample D: slurry was applied on top of the graphite substrate and scratched by hand, rinsed in methanol and dried in vacuum). Wear-tracks were produced in another sample using a diamond stylus leaving a square pattern of 1mm between marks (sample E).

In addition, a pristine graphite surface was etched in a hydrogen plasma (1.5 kW) for 15 min (sample F). Finally, one further sample was Ar ion bombarded at 1 kV for 15 min at a base pressure of 2×10^{-4} mBar using a Gridless End Hall Ion Source (Ion Tech, Inc 3.0-1500-100) (sample G).

Graphite pieces ultrasonically scratched with microdiamond (as described before) were used to study the effect of varying the microwave power during film growth, on the morphology of the resulting films. Microwave powers used were 1.5 (sample H), 3 (sample I) and 3.6 kW (sample J), with a pressure of 133 ± 2 mBar for 2 hours. In order to modify graphite surfaces by introducing oxygen [21-22], three samples ultrasonically scratched with microdiamond were heated at 200°C for 2 days in an oven in atmospheric conditions. These substrates were deposited upon as described above using 1.5 (sample K), 3 (sample L) or 3.6 kW microwave power (sample M), with a pressure of 133 ± 2 mBar for a standard duration of 2 hours.

Diamond films were grown in a stainless steel and quartz 6 kW (2.45 MHz) MPECVD system having a base pressure of $\sim 5 \times 10^{-7}$ mBar, described elsewhere [23]. The plasma was ignited in H_2 and the samples subject to a plasma etch for 15 min prior to the introduction of the CH_4/Ar mixture. During the deposition phase, a mixture of 5% CH_4, 15% H_2 and 80% Ar was excited with 1.5 kW power, with a pressure of 133 ± 2 mBar for 2 hours. After deposition, methane and argon flow was stopped and samples were left with a hydrogen flow for 15 min in order to hydrogenate the surfaces. The substrates were plasma heated and the temperature was measured using a two-colour optical pyrometer to be in the range 850 to 950 °C.

Scanning Electron Microscopy (SEM) analyses were performed in a Hitachi 2700 SEM, operated at 10 keV electron energy, equipped with a secondary electron emission detector. Low magnification (45X) SEM micrographs were analysed to calculate the percentage of area covered by the diamond film on graphite substrates. The analysis was done using a Mat-lab algorithm that counted the pixels corresponding to diamond growth. That is, SEM grayscale

image were transformed to a binary image by replacing all pixels in the grayscale image with luminance greater than a certain level with value 1 and all other pixels with value 0.

Raman spectra (inVia Raman microscope, Renishaw Ltd) were recorded using the 514.5 nm line of an argon ion laser taking the spectra in the range from 200 to 3500 cm^{-1}. X-ray Photoelectron Spectroscopy (XPS) measurements, using Mg K_α X-radiation, were carried out in a Scienta ESCA300 spectrometer at the National Centre for Electron Spectroscopy and Surface Analysis (NCESS) UK. Samples were sputtered with Ar beam at 1 kV energy, and 15-20μA drain current, with ~2.8 x 10^{-6} mbar of Argon to clean surfaces before analysis. This low-energy sputter minimizes graphitisation of the surfaces. Deconvolution of XPS peaks was performed using XPSPeak41 software, using linear background correction and fitted to Gaussian-Lorentzian functions. The XPS peak positions were traceable to an Au standard.

Optical emission spectra of the plasma were measured using a Monolite 6800 spectrometer: spectra were corrected for detector and grating responses using a calibration factor obtained with a near-blackbody tungsten lamp. Spectra were normalized with respect to their highest peak.

3 Results and discussion

Nanocrystalline layers were grown on samples A, B, D, E, F, G, H and K (see Fig. 1a to 1k), all deposited using 1.5 kW power to excite the CH_4-Ar-H_2 gas mixture. The observed "cauliflower-like structure" of these samples has been recently associated with Kardar-Parisi-Zhang who had postulated [24] that the formation of cauliflower-like morphology is due not only to the species attaching to the surface protrusions but also to the growth along the local normal direction**.** The fact that these samples, pre-treated differently, resulted in similar diamond films can be explained by the nucleation mechanism proposed by Dubray *et al.* [25] and Ramesham *et al.* [26] where diamond CVD particles nucleate and grow heteroepitaxially on damaged prism planes of graphite, rather than on diamond debris remaining after scratching.

On the other hand, sample C consists of diamond crystals with submicron sizes and some visible {100} facets (Fig. 1c) in anticipation that Ti may have provided nucleation sites promoting the growth of larger crystals.

Sample I deposited at 3kW presents square microcrystals exhibiting {100} facets with randomly smaller crystals in grain boundaries (Fig. 1i) and sample J deposited at 3.6 kW showed microcrystals with {100} and {111} facets (Fig. 1j). In previously reported work [27] we proposed that the formation of the {100} crystals happens through the formation of steps that by step-flow growth result in terrace formation. At high microwave powers (>3kW), growth rates and hydrogen etching rates are higher. Under these conditions, hydrogen may introduce surface defects that can act as nucleation sites, producing the increase of nucleation density and smaller crystal size. At the higher temperatures (that arise from the higher microwave powers) the morphology changes result in the presence of crystallites with {111} facets.

Annealed sample L (Fig. 1l) showed microcrystals with {111} and {110} facets whereas sample M (Fig. 1m) presented shell-like structures with larger crystals growing perpendicular to the substrate plane. A mechanism for the latter morphology has been proposed by Castro *et al.* [28] where, during diamond growth there is competition for surface sites, that is, growth species may have a higher probability of attaching to the surface protrusions than to surface valleys.

Optical emission spectra of the plasma for all samples are shown in Fig. 2. The emission bands presented are 388, 430 and 776 nm from CH species; 471 and 516 nm are from C_2 Swan band; 656.5, 485 and 436 nm correspond to H_α, H_β and H_γ respectively[3]. The spectra shown in this figure were obtained after 10 min of deposition. All of the nanocrystalline layers grown at 1.5 kW showed high levels of grain re-nucleation caused by the high concentration of C_2 dimers in the chamber [23] (Fig. 2). The production of C_2 is promoted by high pressure conditions (above 100 mbar) and a low concentration of atomic hydrogen.

The intensities, proportional to the concentration of the species in the plasma [29], of the CH bands at 388 and 430 nm are indicative of the diminution of the surface area of the HOPG and the proportional increase in the diamond coverage. Not only do the relative intensities of the CH and C_2 peaks change during deposition (CH peak being higher at the beginning where etching and nucleation take place (seen Fig. 3), but they also depend on the pre-treatment (as shown in Fig. 2).

Raman spectra of all samples (Fig. 4) show typical features of microcrystalline diamond, evidenced by the narrow peak at 1332 cm^{-1} (sometimes obscured by the overlapping D peak) and graphite at ~1342 cm^{-1} and ~1584 cm^{-1} due to the D and G bands. The well-established Raman spectrum of HOPG exhibits a first-order E_{2g} optical mode at 1583 cm^{-1} (G-band), a second order G* peak at 3250 cm^{-1} and a D band at 1370 cm^{-1} from a sample with well-crystallized but small particles. In addition, contributions from sp^2 bonded configurations are revealed at about 1135 cm^{-1} and 1477 cm^{-1}, the latter causing a splitting of the G-band in some samples, or else being obscured by the tail of the G-band. These contributions have been previously attributed to combinations of C=C chain stretching and CH wagging modes of trans-polyacetylene (TPA) chains, which are typically found at the grain boundaries of low quality CVD diamond [30], and the corresponding presence of hydrogen at surface sites. Finally, a second order spectrum shows the D* mode at 2700-2724 cm^{-1}, corresponding to an overtone of the D mode [31].

The fraction of the surface area of the variously prepared samples covered by the diamond film is shown in Table 1. Initial inspection of coatings by low magnification (45X) SEM showed that the percentage of surface covered during deposition varied depending on the nucleation pre-treatment: some are more effective than the control of hydrogen plasma etching and subsequent growth. On the other hand, pre-treatments such as ion bombardment (sample G) and wear tracks (sample E) were less effective compared with the control sample. SEM inspection of the sample pre-treated by wear

3 National Institute of Standards and Technology Atomic Spectra Database, http://physics.nist.gov/PhysRefData/ASD/index.html, (2016)

tracks showed that diamond did not grow on the tracks but on the undamaged substrate areas supporting the idea that diamond grows on graphite prism planes. Ion bombardment may leave behind many terraces on the substrate as has been reported by Hoffman *et al.* [32] on Xe ion irradiation of HOPG but is not translated into a high nucleation density as indicated in Table 1.

The effect of ultrasonic abrasion following surface oxidation appears to provide the optimum conditions for high surface coverage as is shown in Table 1. Without scratching, previous work has shown that HOPG undergoes monolayer pitting when heating in air. The pits arise from natural defects in the basal planes and extend laterally with time due to oxidation of the prism planes. Oxygen decoration of the revealed prism planes, whether arm-chair or zig-zag, is unlikely to influence the nucleation density given the relatively low surface coverage of the pits at the oxidation temperatures adopted in this study. Surface scratching, however, exposes the reactive multilayer prism planes which are potential sites for nucleation and diamond growth.

The XPS spectra of nanocrystalline and polycrystalline layers (Fig. 5) show an intense and sharp C 1s signal at binding energy ~284.4 eV, with typical features indicative of a diamond structure [33, 34]; sp^2 carbon electrons appear at ~283.8 eV and carbon bonded with oxygen (C-O) at ~286 eV (see Fig. 5) [35]. In all cases the carbon sp^3 peak is the highest component (Table 1). XPS analysis of a pristine graphite substrate showed 1.2 at% of oxygen (O 1s peak at binding energy 532 eV, not shown here); after deposition this value was around 1 at% except for the sample G , in which oxygen content was 3.7at%. In the substrates that were heated in air before diamond film deposition, the oxygen content increased to 14.5 at%, and the resulting films showed 1 at% for sample K , 4.8 at% for sample L and 20 at% for sample M. The high oxygen content of surfaces could be enhanced by the production of defective diamond phases and dangling bonds which can rapidly form oxygen functional groups in contact with air after removal from the growth chamber despite a post-growth hydrogen plasma treatment.

4 Conclusions

Graphite and, specifically, highly oriented pyrolytic graphite has been considered a difficult, if not impossible, substrate for PECVD diamond deposition without considerable etching of the graphite. The range of nucleating conditions that have been tested in this work have included manual and ultrasonic scratching, with and without heat treatment in air, plasma and ion etching. We have shown in the present paper that the correct choice of nucleation treatment does enable nanocrystalline and polycrystalline diamond to grow as a continuous film on HOPG. By comparing different treatments prior to microwave PECVD conditions, we have obtained diamond coatings with similar morphology, suggesting that the damaged prism graphite planes, rather than diamond debris resulting from scratching, provide the predominant growth nuclei.

The most uniform growth arose from plasma etching or ultrasonic scratching with micro-diamond. Ultrasonic scratching with a diamond/titanium mixture produced {100} orientated crystallites, whereas oxygenated surfaces generally favoured the formation of {110} and {111} faceted

crystallites. High surface coverage and the best quality polycrystalline diamond (as assessed by SEM, Raman spectroscopy and XPS) resulted from ultrasonic scratching with microdiamond followed by surface oxidation, and using 3kW microwave power during deposition. For nanocrystalline diamond, the preferred treatment was hydrogen plasma etching followed by oxidation using 1.5kW microwave power during deposition.

Acknowledgements

I.V. was supported by CONACYT and by the Programme Alβan, the European Union Programme of High Level Scholarships for Latin America, scholarship No. E05D056416MX. Funding from EPSRC (E/035868/1) is also gratefully acknowledged. Dr. Carlos Torres-Torres for his technical help in the writing of this article and M.C. Victor Valles-Gomez for proof reading the article.

References

[1] S. Porro, G. De Temmerman, D.A. MacLaren, S. Lisgo, D.L. Rudakov, J. Westerhout, M. Wiora, P. John, I. Villalpando, J.I.B. Wilson, Diam. Relat. Mater. **19**, 818 (2010)

[2] C.J. Tang, A.J. Neves, A.J.S. Fernandes, Diamond Relat. Mater. **12**, 1488 (2003)

[3] D. Das, R. N. Singh, Int. Mater. Rev. **52**, 29 (2007)

[4] Y.C. Chu, Y. Tzeng, O. Auciello, J. Appl. Phys. **115**, 024308 (2014)

[5] C.J. Tang, A.J.S. Fernandes, A.V. Girao, S. Pereira, Fa-Nian Shi, M.R. Soares, F. Cossta, A.J. Neves, J.L. Pinto, J. Cryst Growth. **389**, 83 (2014)

[6] R. Haubner, W. Kalss, Int. J. Met. Hard Mater. **28**, 475 (2010)

[7] S. Porro, G. De Temmerman, S. Lisgo, P. John, I. Villalpando, J.W. Zimmer, B. Johnson, J.I.B. Wilson, Diamond Relat. Mater. **18**, 740 (2009)

[8] S. Porro, G. De Temmerman, P. John, S. Lisgo, I. Villalpando, J.I.B. Wilson, Phys. Status Solidi A. **206**, 2028 (2009)

[9] G. De Temmerman, R.P. Doerner, P. John, S. Lisgo, A. Litnovsky, L. Marot, S. Porro, P. Petersson, M. Rubel, D.L. Rudakov, G. Van Rooij, J. Westerhout, J.I.B. Wilson, Phys. Scr. **T138**, 014013 (2009)

[10] M. Volmer, A. Weber. Z. Phys. Chem. **119**, 277 (1926)

[11] C.C. Battaile, D.J. Srolovitz, I.I. Oleinik, D.G. Pettifor, A.P. Sutton, S.J. Harris, J.E. Butler, J. Chem. Phys. **11**, 4291 (1999)

[12] W. R.L. Lambrecht, C.H. Lee, B. Segall, J.C. Angus, Z.Li, M. Sunkara, Nature, **364**, 607 (1993)

[13] S.P. Mehandru, A.B. Anderson, J.C. Angus, J. Phys Chem. **96**, 10978 (1992)

[14] Z. Li, L. Wang, T. Suzuki, A. Argoitia, P. Pirouz, J. C. Angus, J. Appl. Phys. **73**, 711 (1993)

[15] L. Chow, H. Wang, S. Kleckley, A. Shulte, K. Casey, Solid State Commun, **93**, 999 (1995)

[16] L.L. Regel, W.R. Wilcox, J.Mater. Sci. Lett. **19**, 455 (2000)

[17] L. Cong, W. Jianhua, L. Sijia, X. Liwei, W. Jun, C. Xiaohui, Plasma Sci. and Tech. **17**, 496 (2015)

[18] J.G. Buijnsters, P. Shankar, W.J.P. van Enckevort, J.J. Schermer, J.J. ter Meulen, Phys. Status Solidi A. **195**, 383 (2003)

[19] S.P. Bozeman, B.R. Stoner, J.T. Glass, in Handbook of Industrial Diamonds and Diamonds Films, ed. M.A. Prelas, G. Popovici, L.K. Bigelow (Marcel Dekker, New York,1998), p. 901

[20] T. Jiang and K. Xu, Carbon **33**, 1663 (1995)

[21]P. John, N. Polwart, C.E. Troupe and J.I.B. Wilson, Diamond Relat. Mater. **11**, 861 (2002)

[22] N. Polwart, PhD thesis, Heriot-Watt University, Edinburgh UK, 2003

[23] J.R. Rabeau, P. John, J.I.B. Wilson and Y. Fan, J. Appl. Phys. **96**, 6724 (2004)

[24] V. Podgursky, A. Bogatov, V. Sedov, I. Sildos, A. Mere, M. Viljus, J.G. Buijnsters, V. Ralchenko, Diamond Relat. Mater. **58**, 172 (2015)

[25] J. J. Dubray, C. G. Pantano, W. A. Yarbrough, J. Appl. Phys. **72**, 3136 (1992)

[26] R. Ramesham, R. F. Askew, M. F. Rose, B. H. Loo, J. Electrochem. Soc. **140**, 3018 (1993)

[27] I. Villalpando, P.John, S.Porro and J.I.B. Wilson, Diamond Relat. Mater. **20,** 711 (2011)

[28] M. Castro, R. Cuerno, M. Nicoli, L. Vazquez and J. G. Buijnsters, New J. Phys. **14**, 103039 (2012)

[29] P. John, J.R. Rabeau, J.I.B. Wilson, Diamond Relat. Mater. **11**, 608 (2002)

[30] A.C. Ferrari and J. Robertson, Phys. Review B, **63**, 121405 (2001)

[31] S. Reich and C. Thomsen, Phil. Trans. R. Soc. A, **362**, 2271 (2004)

[32] A. Hoffman, A. Fayer, A. Laikhtman, R. Brener, J. Appl. Phys. **77,** 3126 (1995)

[33] A. Cook, A.G. Fitzgerald, A.G. Storey, J.I.B. Wilson, P. John, M.G. Jubber, D. Milne, I. Drummond, J.A. Savage, S. Haq, Diamond Relat. Mater. **1**, 478 (1992)

[34] J.I.B. Wilson, J.S.Walton, G. Beamson, J. Electron Spectroscopy. Relat. phenom. **121**, 183 (2001)

[35] G. Beamson and D. Briggs, (Wiley, New York, 1992), p. 112.

Figure Captions

Fig. 1 SEM micrograph of the deposited films, a) and b) correspond to samples A and B showing, cauliflower-like structure; c) sample C, with diamond crystals with submicron sizes and some visible {100} facets; d) to h) Samples D to H, presenting cauliflower-like structure; i) sample I with square microcrystals exhibiting {100} facets with randomly smaller crystals in grain boundaries; j) sample J, presenting microcrystals with {100} and {111} facets; k) sample K with cauliflower-like structure; l) Sample L, showing microcrystals with {111} and {110} facets; finally, m) Sample M, presenting shell-like structures with larger crystals growing perpendicular to the substrate plane

Fig. 2 Optical emission spectroscopy for all samples after ten minutes of MPECVD

Fig. 3 Optical emission spectroscopy for sample C showing the change in relative intensities of the CH and C_2 peaks

Fig. 4 Raman analysis of samples a)A, b)B, c)C, d)D, e)E, f)F, g)G, h)H, i)I, j)J, k)K, l)L and m)M showing typical features from TPA at ~1135cm^{-1}, diamond at ~1333cm^{-1}, D-band at ~1340cm^{-1}, G-band at ~1584 cm^{-1} and D*-band at ~2700 cm^{-1}

Fig 5 XPS spectra of all the prepared samples, green line shows deconvolution of XPS spectrum sample A

Table 1 Percentage of surface covered by MPECVD diamond for the pre-treated graphite substrates and sp^3/sp^2 ratio determined by XPS

Table 1 Percentage of surface covered by MPECVD diamond for the pre-treated graphite substrates

Sample label	Treatment	Heated in a box oven	Microwave power (kW)	Surface covered (%) determined by SEM	sp^3/sp^2 ratio determined by XPS
A.	Control sample	No	1.5	68±9	30±3
B.	Ultrasonically Scratched with nanodiamond	No	1.5	46±5	23±2
C.	Ultrasonically Scratched with microdiamond +Ti	No	1.5	69±8	39±4
D.	Manually scratched with microdiamond	No	1.5	55±7	33±3
E.	Wear tracks	No	1.5	24±3	50±5
F.	Plasma etching	No	1.5	92-11/+8	21±2
G.	Ion bombardment	No	1.5	56±7	51±5
H.	Ultrasonically Scratched with microdiamond	No	1.5	78±9	48±5
I.	Ultrasonically Scratched with microdiamond	No	3.0	97-12/+3	81±8
J.	Ultrasonically Scratched with microdiamond	No	3.6	87±10	40±4
K.	Ultrasonically Scratched with microdiamond	Yes	1.5	99-12/+1	40±4
L.	Ultrasonically Scratched with microdiamond	Yes	3.0	93-11/+7	81±8
M.	Ultrasonically Scratched with microdiamond	Yes	3.6	99-12/+1	40±4

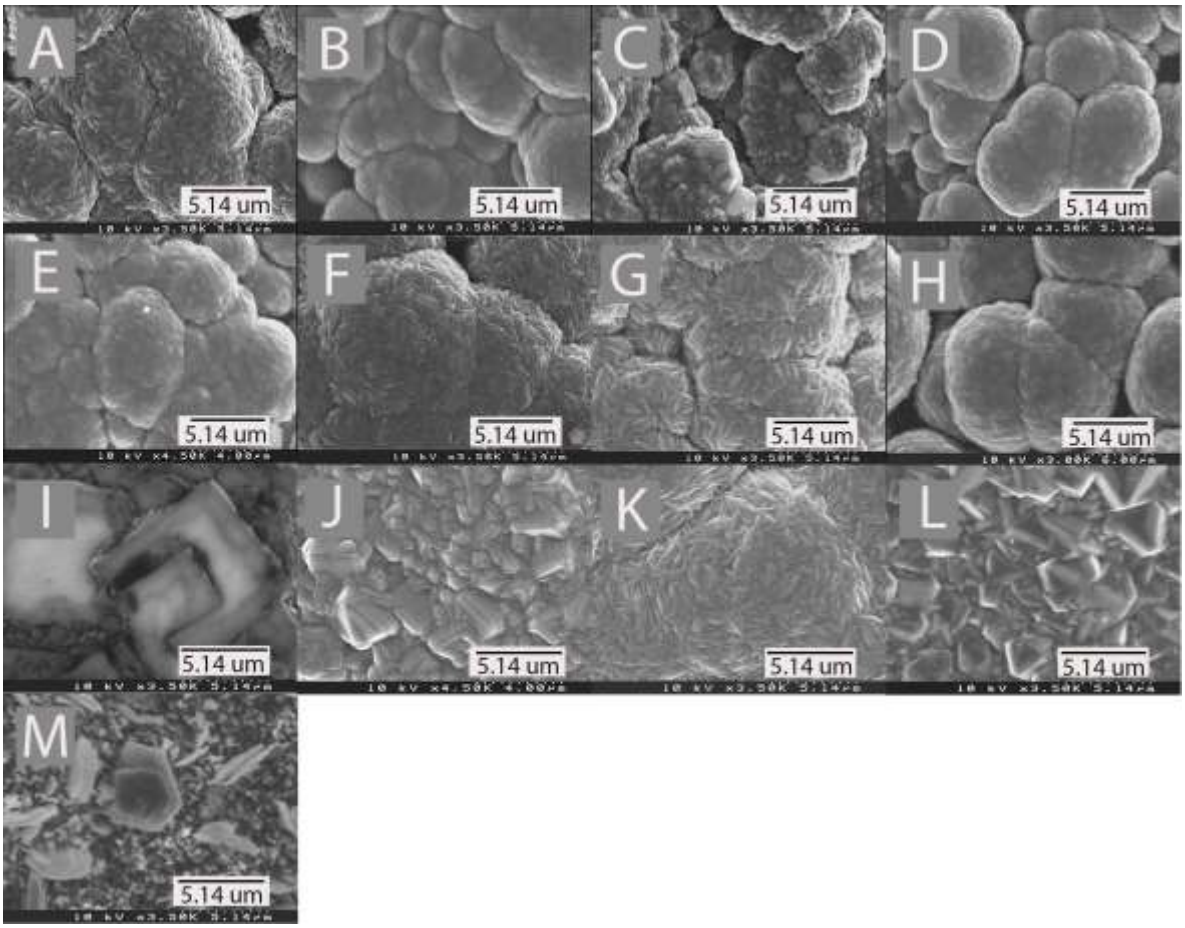
A
5.14 um
B
5.14 um
C
5.14 um
D
5.14 um
E
5.14 um
F
5.14 um
G
5.14 um
H
5.14 um
I
5.14 um
J
5.14 um
K
5.14 um
L
5.14 um
M
5.14 um

Figure 1

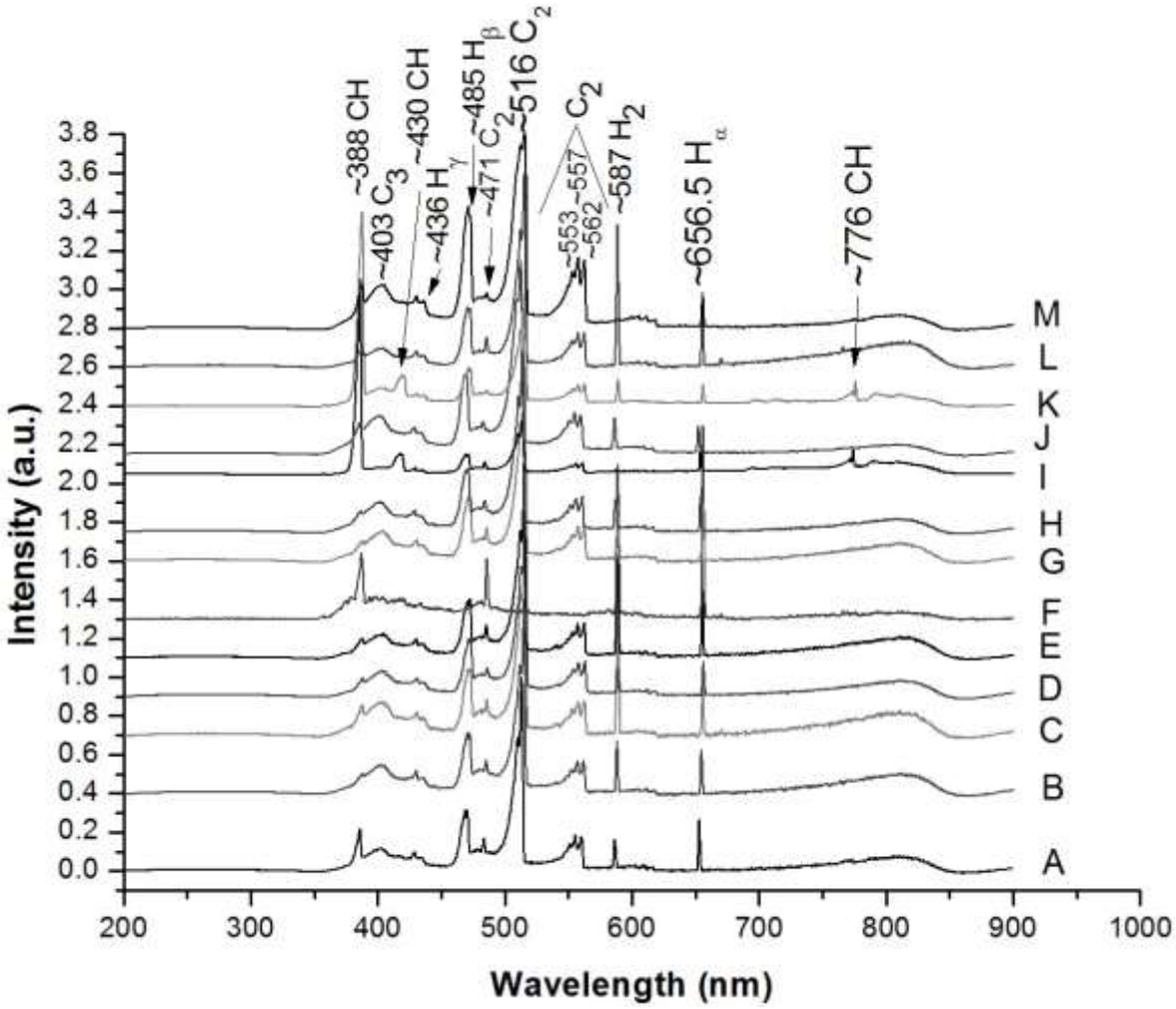
~388 CH
~403 C3
~430 CH
~436 Hγ
~485 Hβ
~471 C2
~516 C2
C2
~553
~557
~562
~587 H2
~656.5 Hα
~776 CH
M
L
K
J
I
H
G
F
E
D
C
B
A
Intensity (a.u.)
Wavelength (nm)
0.0
0.2
0.4
0.6
0.8
1.0
1.2
1.4
1.6
1.8
2.0
2.2
2.4
2.6
2.8
3.0
3.2
3.4
3.6
3.8
200
300
400
500
600
700
800
900
1000

Figure 2

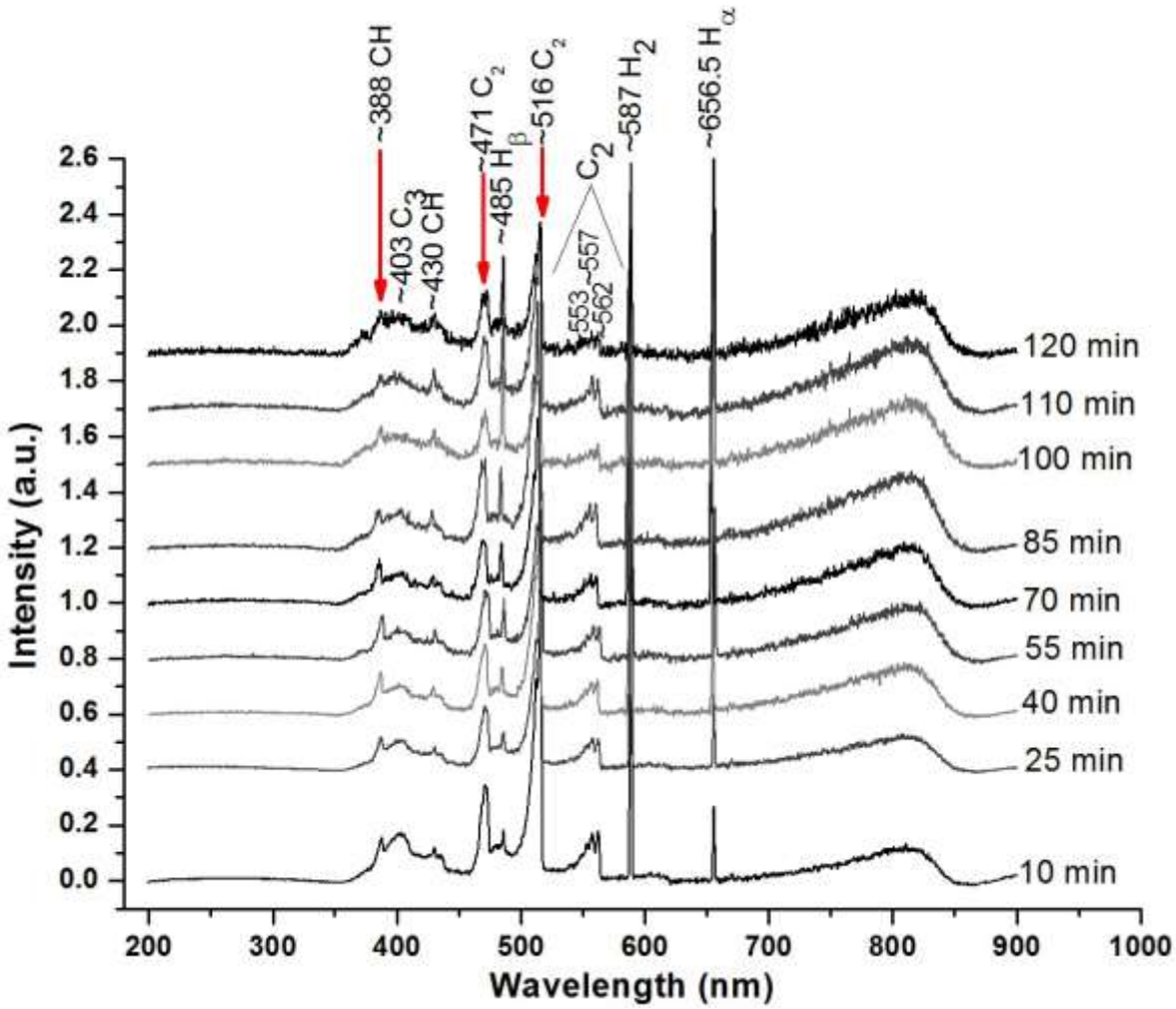
~388 CH
~403 C3
~430 CH
~471 C2
~485 Hβ
~516 C2
C2
~553
~557
~562
~587 H2
~656.5 Hα
120 min
110 min
100 min
85 min
70 min
55 min
40 min
25 min
10 min
Intensity (a.u.)
Wavelength (nm)
0.0
0.2
0.4
0.6
0.8
1.0
1.2
1.4
1.6
1.8
2.0
2.2
2.4
2.6
200
300
400
500
600
700
800
900
1000

Figure 3

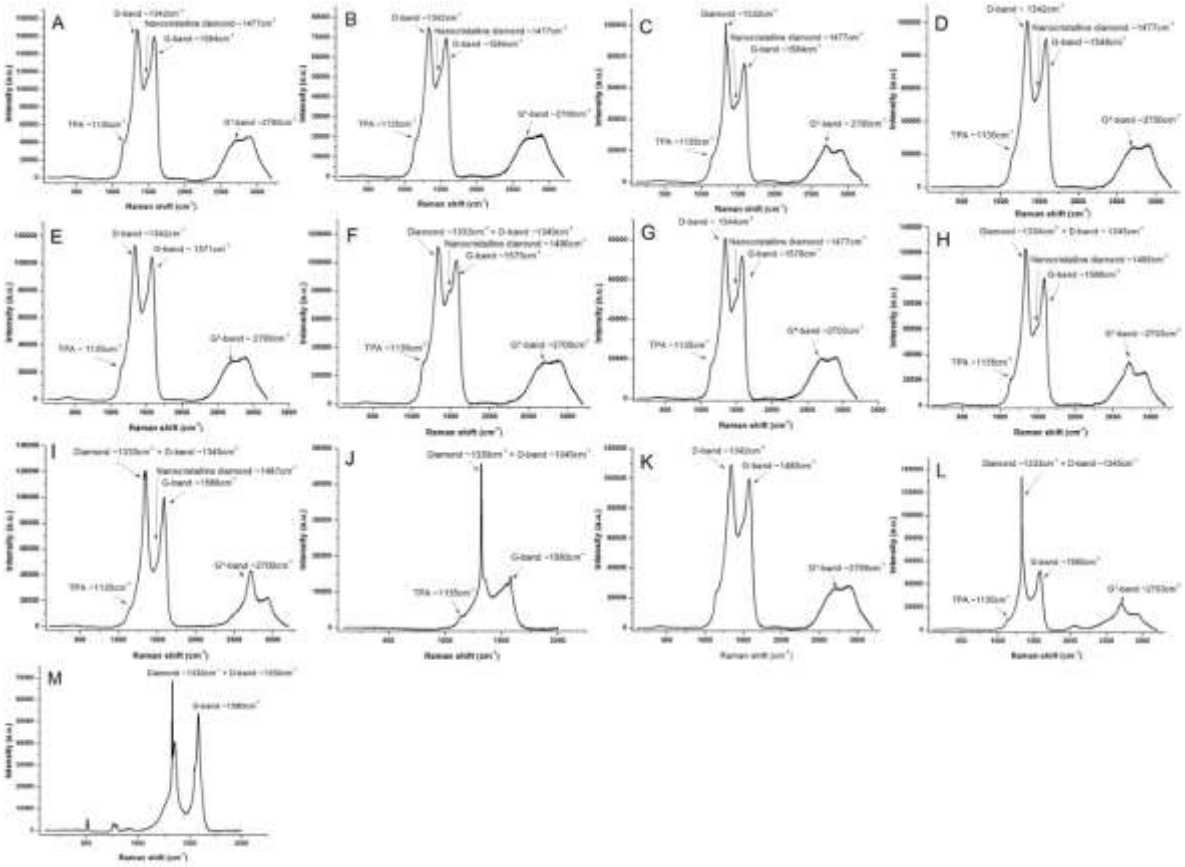

Figure 4

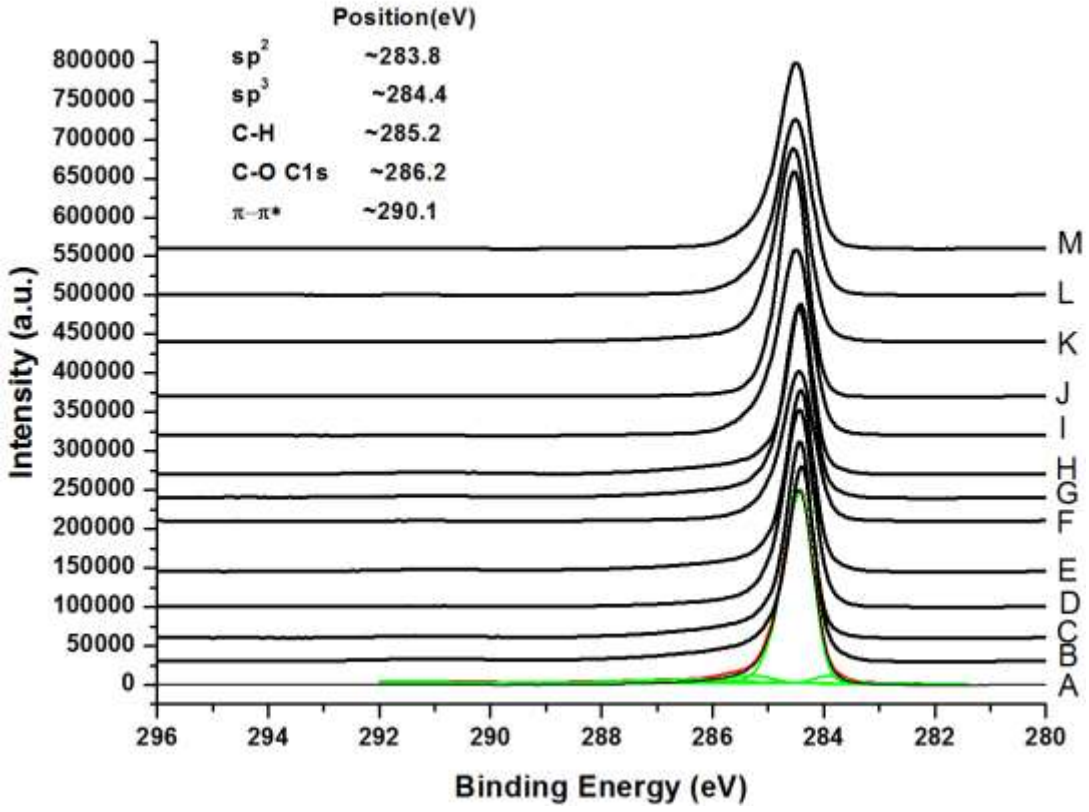
Position(eV)
sp2 ~283.8
sp3 ~284.4
C-H ~285.2
C-O C1s ~286.2
π–π* ~290.1
Intensity (a.u.)
800000
750000
700000
650000
600000
550000
500000
450000
400000
350000
300000
250000
200000
150000
100000
50000
0
296
294
292
290
288
286
284
282
280
Binding Energy (eV)
M
L
K
J
I
H
G
F
E
D
C
B
A

Figure 5